

# Mesopore Formation in USY and Beta Zeolites by Base Leaching: Selection Criteria and Optimization of Pore-Directing Agents

**Journal Article****Author(s):**

Verboekend, Danny; Vilé, Gianvito; Pérez-Ramírez, Javier

**Publication date:**

2012-06-06

**Permanent link:**

<https://doi.org/10.3929/ethz-a-010788570>

**Rights / license:**

[In Copyright - Non-Commercial Use Permitted](#)

**Originally published in:**

Crystal Growth & Design 12(6), <https://doi.org/10.1021/cg3003228>

**Funding acknowledgement:**

134572 - A fundamental approach to the scale up of hierarchical zeolite catalysts (SNF)

# Mesopore formation in USY and beta zeolites by base leaching: selection criteria and optimization of pore-directing agents

*Danny Verboekend, Gianvito Vilé, and Javier Pérez-Ramírez\**

Institute for Chemical and Bioengineering, Department of Chemistry and Applied Biosciences, ETH Zurich, Wolfgang-Pauli-Strasse 10, CH-8093, Zurich, Switzerland.

\* Corresponding author. E-mail: [jpr@chem.ethz.ch](mailto:jpr@chem.ethz.ch).

## **Abstract**

Molecular criteria for the selection of organic pore-directing agents (PDAs) in NaOH leaching, that is desilication, were investigated on USY and beta zeolites of distinct aluminum contents (Si/Al = 15-385). PDAs prove particularly useful for FAU and BEA topologies since they serve a dual purpose: tailoring the mesopore structure while preventing realumination and amorphization of the crystals. A comprehensive approach revealed that an efficient PDA is positively charged and contains *ca.* 10-20 carbon atoms, *e.g.* TPA<sup>+</sup> or CTA<sup>+</sup>. Compositional, textural, morphological, structural, and acidity studies performed on selected hierarchical zeolites confirmed the presence of extensive secondary porosity coupled to well-preserved zeolitic properties. Inclusion of TPA<sup>+</sup> in the alkaline solution led to the largest preservation of the intrinsic zeolite properties, whereas CTA<sup>+</sup> facilitates the reassembly of dissolved species during alkaline treatment. Finally, we report the first-time synthesis of mesoporous zeolites in a continuous-mode preparation using a tubular reactor and a continuous stirred-tank reactor, attaining reactor productivities up to 100 times that of conventional batch preparation.

**Keywords:** Hierarchical Zeolites; USY; Beta; Desilication; Tetraalkylammonium cations; Surfactants.

## 1. Introduction

Zeolites represent the most important family of catalysts in the petrochemical and oil refining industries. Nevertheless, although they possess an impressive array of exceptional features, their narrow micropores (*ca.* 0.5-1 nm) often imply transport limitations of reactants and products, compromising a full utilization of the active sites [1,2]. As a response, for over a decade now, an intense and persistent scientific attention focused on increasing the accessibility of the zeolite's active sites by widening of the micropore channels [3], reducing the zeolite crystal size by one or multiple dimensions [4,5], or by introducing intra-crystalline mesopores in the zeolite crystals [6,7]. The latter two groups of materials complement the intrinsic zeolite microporosity with a secondary (meso)porosity giving rise to the class of hierarchical zeolites. The auxiliary pore structure aims at enhancing, much like the venal systems in many larger organisms, molecular transport to and from the active sites, ultimately leading to an improved catalytic performance [8-10].

Desilication, or base leaching, is an effective, affordable, and scalable approach to introduce interconnected mesopores in zeolite crystals. In addition, desilication can be applied to a wide variety of structures and compositions. Base treatment, classically performed in aqueous NaOH, leads to the dissolution of both Al and Si species from the framework. However, extracted Al species realuminate on the zeolite's external surface, lowering the Si/Al ratio of the resulting solid. Since the latter process also regulates intra-crystalline mesopore formation, aluminum was coined pore-directing agent [7].

One promising variant to the classical NaOH treatment comprises the use of an organic base, *e.g.* tetraalkylammonium (TAA) hydroxides, as it leads to better preserved intrinsic zeolitic properties, *e.g.* crystallinity and microporosity [11-13]. Moreover, in the case of ZSM-5, using mixtures of NaOH and TPAOH enabled to moderate mesopore growth, yielding high-hierarchy factor zeolites, *i.e.* those combining high microporosity and mesoporosity [12]. A similar approach on Al-deficient silicalite-1 proved that, besides trivalent framework cations, TAAs also actively function as pore-direction agent, enabling the synthesis of hierarchical all-silica zeolites by desilication [14]. Nevertheless, optimization of the TAA concentration at constant alkalinity was thus far limited to relatively stable MFI zeolites.

The efficiency of a tetraalkylammonium cation in desilication depends strongly on its affinity to the zeolite surface [14]. Still, only common quaternary ammonium cations, used in zeolite synthesis, were explored for this purpose, *e.g.* tetrapropylammonium (TPA<sup>+</sup>) and tetramethylammonium (TMA<sup>+</sup>). Likely, other molecules used in zeolites synthesis exert the same, or an even superior effect. For example, cetyltrimethylammonium (CTA<sup>+</sup>), frequently used as a secondary (mesopore) template in the synthesis of hierarchical zeolites [15,16], should display a distinct affection to the zeolite under alkaline conditions. Particularly interesting is that the presence of CTA<sup>+</sup> in alkaline solutions containing fully-dissolved zeolite species gives rise to the formation of MCM-41-type mesoporous materials with strong Brønsted acidity [17]. Moreover, the presence of CTA<sup>+</sup> in combination with fully- *and* partially-dissolved zeolites species can lead to the formation of zeolite/MCM-41 composites [18] or to a surfactant-induced reassembly [19-21].

Herein, we evaluate the role of a variety of organic molecules in desilication to develop general criteria for suitable pore-directing agents. Their efficiency is examined in the preparation of hierarchical USY and beta zeolites, which strongly benefit from the presence of PDAs in the NaOH solution. It is shown that a wide variety of quaternary ammonium cations and amines positively influence the desilication of these structures, the impact of which depending on their charge and size. The type and concentration of pore-directing agents enable to tune the external (mesopore) surface, pore size, and also to minimize amorphization. Moreover, the inclusion of PDAs permits to prevent realumination during desilication, yielding solids with Si/Al ratios similar to that of the starting zeolite. The properties of selected hierarchical zeolites is demonstrated by an extended characterization, including ICP-OES, XRD, TEM, SEM, N<sub>2</sub> and Ar sorption, He pycnometry, and FT-IR spectroscopy. We show that TPA<sup>+</sup> yields mesoporous solids with the highest zeolitic properties, whereas CTA<sup>+</sup> gives rise to a reassembly of dissolved species. Finally, we present for the first time strategies for continuous preparation of mesoporous zeolites by base leaching.

## 2. Experimental

*Materials and procedures:* The parent USY zeolites, supplied by Zeolyst International (CBV720 Si/Al = 15 and CBV760 Si/Al = 30) and TOSOH (390HUA Si/Al = 385), were coded 'USY $x$ ', where ' $x$ ' represents the nominal Si/Al ratio. The parent beta zeolite, coded 'beta220', was supplied by TOSOH (890HOA, Si/Al = 220). These zeolites were in the protonic form. The NaY zeolite, purchased from Zeolyst International (CBV100 Si/Al = 2.4, coded 'Y2.4'), represents the mother Y zeolite from which USY15 and USY30 were derived. The above-mentioned codes were only used in the case reference was made to a zeolite other than USY30. The starting zeolites were generically referred to with the code 'P' (parent). Nanopowdered amorphous silica (SiO<sub>2</sub>) and high surface area alumina (Al<sub>2</sub>O<sub>3</sub>) were supplied by Sigma-Aldrich and Alfa Aesar, respectively. NaOH (97%) and PDAs ( $\geq$  97%), used in the alkaline treatments, were provided by chemical suppliers as Fluka, Sigma-Aldrich, Alfa Aesar, and Acros.

Alkaline-treated samples in aqueous NaOH were labeled AT. When a PDA was included in the alkaline solutions, 'AT' was followed by the PDA's acronym (as defined in **Table 1**) and the applied molar concentration (' $c$ '). For conciseness, the charge of the PDAs was omitted in sample labeling. When reference was made to PDA-containing uncalcined samples, 'uncalcined' was added to the sample code. Most treatments were performed batchwise using a Mettler Toledo Easymax 102 reactor system (**Fig. 1a**). In a typical experiment, the alkaline solution (0.2 M NaOH +  $c$  PDA) was stirred at 500 rpm and heated to 338 K, after which the zeolite sample (3.3 g of zeolite per 100 cm<sup>3</sup> of solution) was introduced. The resulting suspension was left to react for 30 min, followed by quenching, filtration, extensive washing using distilled water, and overnight drying at 338 K. Finally, the obtained powder was calcined in air at 823 K for 5 h, at a heating rate of 5 K min<sup>-1</sup>. Samples were weighed before and after calcination to determine the amount of PDA remaining on the dried solid. The latter value was corrected for adsorbed water (*ca.* 10 wt.%).

Continuous-mode desilication was performed using either a relatively long tubular reactor at 338 K (**Fig. 1b**) or a high-shear micro-reactor at 298 K (IKA Ultra Turrax T25, **Fig. 1c**). In both

configurations, two peristaltic pumps were used to co-feed an aqueous solution of NaOH (0.4 or 0.8 M) and TPABr (0.1 M) and a zeolite slurry (6.6 g of zeolite per 100 cm<sup>3</sup> water) at room temperature into the reactors. The samples were quenched at the reactor outlet and filtered as described for the conventional batch treatment.

In some cases, the samples were brought in the protonic form by 3 consecutive ion exchanges in 0.1 M NH<sub>4</sub>NO<sub>3</sub> (298 K, 8 h, 1 g zeolite per 100 cm<sup>3</sup> of solution), followed by calcination according to the above-mentioned protocol.

*Characterization:* Powder X-ray diffraction (XRD) patterns were acquired in a PANanalytical X'Pert PRO-MPD diffractometer equipped with Bragg-Brentano geometry and Ni-filtered Cu K $\alpha$  radiation ( $\lambda = 0.1541$  nm). Data were recorded in the  $2\theta$  range of 3-60° with an angular step size of 0.05° and a counting time of 8 s per step. The relative crystallinity was estimated from the intensity of the (533) reflection at 24°  $2\theta$ , assuming a nominal 100% crystallinity in the parent USY30. Si and Al concentrations in the solids were determined by inductively coupled plasma optical emission spectroscopy (ICP-OES) on a Horiba Ultima 2 instrument equipped with photomultiplier tube detection. C, H, and N concentrations in the solids were attained by quantitative infrared spectroscopy performed using a LECO CHN-900 combustion furnace. Scanning electron microscopy (SEM) was carried out using a LEO Gemini 1530 microscope operated at 1 kV. Transmission electron microscopy (TEM), and selected area electron diffraction (SAED) were performed using a FEI Tecnai F30 microscope operated at 100 kV. Nitrogen sorption at 77 K was carried out in a Quantachrome Quadrasorb-SI instrument. Prior to the measurement, the samples were degassed in vacuum at 573 K for 3 h. The  $t$ -plot method was used to discriminate between micro- and mesoporosity. The mesopore size distribution was obtained by the Barrett-Joyner-Halenda (BJH) model applied to the adsorption branch of the isotherm. High-resolution low-pressure Ar adsorption isotherms were recorded at 87 K and 77 K on a Micromeritics ASAP 2020 analyzer after *in situ* pretreatment at 623 K for 8 h. The hybrid non-linear density functional theory (NLDFT) model describing argon adsorption in cylindrical micro- and mesopores was used to calculate the pore size distribution. Skeletal densities of the solids were obtained

by He pycnometry performed on a Micromeritics Accupyc II 1340 instrument. Prior to analysis, the samples (*ca.* 300 mg) were dried in vacuum at 373 K for 4 h. The density was obtained by taking the average of 50 measurements after equilibration for 150 measurements. Fourier transform infrared (FTIR) spectroscopy was carried out in a Thermo Nicolet 5700 spectrometer equipped with a SpectraTech Collector II diffuse reflectance (DRIFTS) accessory and a high-temperature cell, KBr windows, and an MCT detector. Spectra were recorded under a nitrogen atmosphere at 473 K, in the range of 650-4000  $\text{cm}^{-1}$ , by co-addition of 200 scans and with a nominal resolution of 4  $\text{cm}^{-1}$ . Prior to the measurement, the samples were dried at 573 K in flowing  $\text{N}_2$  (100  $\text{cm}^3 \text{min}^{-1}$ ) for 60 min.

### 3. Results and discussion

The majority of the alkaline treatments were performed on a commercial USY zeolite that was previously severely steamed and acid leached, *i.e.* USY30. In Section 3.1, a wide variety of organic compounds is examined for pore-directing capabilities in the NaOH leaching of this specific zeolite. In Section 3.2, the concentration effect of selected PDAs ( $\text{TMA}^+$ ,  $\text{TPA}^+$ , and  $\text{CTA}^+$ ) in alkaline treatment of the USY30 sample is studied, while Section 3.3 describes the characterization of selected USY30 zeolites in more detail. Section 3.4 deals with the influence of the aluminum content in differently dealuminated USY zeolites (USY15, USY30, and USY385), as well as application to zeolite beta (beta220). Finally, Section 3.5 covers approaches for the continuous synthesis of hierarchical zeolites.

#### 3.1. Screening of PDAs in base leaching

The candidates for pore direction during desilication were screened on USY30 with  $\text{Si}/\text{Al} = 37$ , which was referred to as the parent (P) zeolite. XRD analysis revealed that this zeolite featured solely the faujasite diffraction pattern (**Fig. 2a**). SEM evidenced aggregated octahedron-type faujasite crystals containing large mesopores, which should have originated during dealumination of the pristine Y zeolite by steaming and acid leaching (**Fig. 3**) [22]. TEM confirmed the crystalline character of the crystals (**Fig. 4**) and the presence of large mesopores and macropores (not shown). Additionally, particularly



visible at the crystal edges, the micrographs of P contained amorphous species, most likely originated during the steaming and acid leaching steps (**Fig. 4**) [23]. The N<sub>2</sub> isotherm displayed a large uptake at low relative pressures combined with a limited uptake at  $p/p_0 > 0.1$  (**Fig. 5a**, open circles). Accordingly, a micropore volume ( $V_{\text{micro}}$ ) of 0.33 cm<sup>3</sup> g<sup>-1</sup> and a mesopore surface area ( $S_{\text{meso}}$ ) of 117 m<sup>2</sup> g<sup>-1</sup> were accounted for (**Table 2**). Prior to adding any PDA to the alkaline solution, the influence of 0.2 M NaOH treatment was examined (AT). Upon desilication, SEM evidenced a similar morphology as well as more numerous and slightly larger meso- and macropores (**Fig. 3**). XRD (**Fig. 2a**) and TEM (**Fig. 4**) demonstrated a severe sample amorphization. The corresponding N<sub>2</sub> isotherm displayed little uptake at  $p/p_0 < 0.1$ , whereas uptake at higher pressures increased substantially (**Fig. 5a**, black circles). Therefore, although the external surface of the material exceeded 300 m<sup>2</sup> g<sup>-1</sup> and a centered mesopore size ( $d_p$ ) of ~5 nm was obtained (**Fig. 5c**), the micropore volume, reduced to zero (**Table 2**). Accordingly, judging by the complete lack of crystallinity and microporosity, treatment in NaOH alone is definitely not a suitable approach to obtain hierarchical USY zeolites.

The efficiency of the possible pore-directing agents in desilication was (preliminarily) determined by examination of the solid yield of the treatment and porosities of the resulting solids (**Table 2**). Using the desilication efficiency (DE) [24] the introduced mesoporosity was coupled to the weight loss upon the treatment. Moreover, using the indexed hierarchy factor (IHF) [25], the intrinsic zeolite properties (represented by  $V_{\text{micro}}$ ) and the amount of the auxiliary mesoporosity (represented by  $S_{\text{meso}}$ ) were combined to rank the porous architectures in a more quantitative manner. For this purpose, the micropore and mesopore volumes were normalized by the maximum values, *i.e.*  $V_{\text{micro}} = 0.33 \text{ cm}^3 \text{ g}^{-1}$  (P) and  $S_{\text{meso}} = 733 \text{ m}^2 \text{ g}^{-1}$  (AT-DSA-0.2), and factored yielding the overall formula:  $\text{IHF} = (V_{\text{micro}} / 0.33 \text{ cm}^3 \text{ g}^{-1}) \times (S_{\text{meso}} / 733 \text{ m}^2 \text{ g}^{-1})$ .

Unlike could be expected based on the marked differences on the yield in PDA-mediated desilication on silicalite-1 [14], the yields after the treatments (with or without 0.2 M of PDA) were relatively similar (*ca.* 40-60%). This is attributed to the lower FAU framework density [26], facilitating dissolution in alkaline media. The negatively charged surfactant (DS<sup>-</sup>) did not lead to an improved

desilication;  $V_{\text{micro}}$ , hence IHF, was zero and  $S_{\text{meso}}$  was limited to  $144 \text{ m}^2 \text{ g}^{-1}$ . The non-ionic species (P123 and amines) did affect the leaching process positively. Solids with increased micropore volumes (up to  $0.17 \text{ cm}^3 \text{ g}^{-1}$  for DEA) and mesopore surface areas (up to  $498 \text{ m}^2 \text{ g}^{-1}$  for DAH) were obtained. Particularly the amines, common structure-directing agents in the synthesis of unidirectional zeolites [27], proved able to enhance mesoporosity substantially, while largely preserving the microporosity. The latter should be due to their distinct affinity to the zeolite micropores under alkaline conditions [28]. Nevertheless, only the solid treated in the presence of DEA displayed an IHF significantly superior (0.34) to that of the parent (0.16).

Alkylammonium cations were highly suitable pore-directing agents, supporting that the electrostatic affinity to the zeolite is a decisive factor [14]. Micropore volumes up to  $0.28 \text{ cm}^3 \text{ g}^{-1}$  ( $\text{TPA}^+$ ) were combined with external surfaces up to  $733 \text{ m}^2 \text{ g}^{-1}$  ( $\text{DSA}^+$ ), and all associated IHFs largely exceeded that of the parent sample.  $\text{TPA}^+$  revealed the highest IHF (0.67) as it combined a  $V_{\text{micro}}$  of  $0.28 \text{ cm}^3 \text{ g}^{-1}$  to an external surface of  $578 \text{ m}^2 \text{ g}^{-1}$ , *i.e.* a five-fold that of the parent USY. In line with previous observations [13], the desilication efficiencies were relatively high. Whereas PDA-assisted base leaching boosted efficiencies up to  $8 \text{ m}^2 \text{ g}^{-1} \%^{-1}$  for MFI [7], **Table 2** contains values up to *ca.*  $12 \text{ m}^2 \text{ g}^{-1} \%^{-1}$ . These higher values are attributed to the lower FAU framework density. A variety of mesopore sizes ( $d_p$ ) were obtained (3-12 nm), enabling to tailor the porosity by PDA selection. Unlike in the case of all other PDAs, a very narrow mesopore size distribution was obtained when NaOH leaching was conducted in the presence of  $\text{CTA}^+$ . Accordingly,  $\text{CTA}^+$ -derived samples were thoroughly characterized in Sections 3.2 and 3.3. The alkylammonium cations comprising less than *ca.* 10 carbon atoms ( $\text{TMA}^+$ ,  $\text{PTA}^+$ , and  $\text{TEA}^+$ ) protected the micropore volume less effectively. This is tentatively attributed their fewer or shorter alkyl chains, not able to form a closely packed adsorption layer [29]. The latter should in turn yield a less efficient protection. PDAs with more than *ca.* 20 carbon atoms, *e.g.*  $\text{DSA}^+$  and  $\text{BE}^+$ , should be considered less attractive due to solubility and calcination impracticalities. Hence, an efficient PDA in desilication features a cationic charge and alkyl moieties in the range of *ca.* 10-20 carbon atoms.

### 3.2. Influence of PDA concentration

The effect of concentration ( $c$ ) was studied on yield, porosity, crystallinity, and Si/Al ratio for TPA<sup>+</sup>, TMA<sup>+</sup>, and CTA<sup>+</sup>. The N<sub>2</sub> isotherms of AT-CTA-0.2 and P showed a similar uptake at low relative pressures (**Fig. 5a**). On the other hand, the isotherms of AT-TPA-0.2 displayed an enhanced uptake at  $p/p_0 < 0.1$ , whereas that of AT-TMA-0.2 exhibited only about 60% of the uptake of P. At  $p/p_0 > 0.1$ , both AT-TPA-0.2 and AT-CTA-0.2 evidenced strongly enhanced uptake, compared to P and AT. On the other hand, the uptakes of AT-TMA-0.2 and AT were fairly similar. The mesopore size distributions of AT, AT-TMA-0.2, and AT-TPA-0.2 were centered around 5, 4, and 7 nm, respectively (**Fig. 5c**). These pore size distributions, and those of alkaline-treated zeolites in general [7], are typically not as well defined as those obtained by organosilane-directed synthesis [30] or by surfactant-induced reassembly [21]. Therefore, the very sharp mesopore size distribution of AT-CTA-0.2, centered at 3.7 nm, suggests that a reassembly of dissolved species could have taken place during alkaline treatment (*vide infra*).

Generally, the yields increased with the concentration of PDA, which is attributed to the inhibition of the zeolite dissolution by the adsorption of these cationic species on the external surface. However, for CTA<sup>+</sup> and TPA<sup>+</sup> at concentrations  $> 0.1$  M, yields reduced (**Fig. 6a**). The amount of adsorbed pore-directing agent (PDA<sub>ads</sub>) evidenced a clear relation with the concentration of PDA in solution. **Fig. 6b** shows that at 0.2 M, the amounts adsorbed for both TMA<sup>+</sup> and TPA<sup>+</sup> (*ca.* 10 wt.%) were much lower than that for CTA<sup>+</sup> (*ca.* 40 wt.%).

Selected PDA-containing uncalcined samples, *i.e.* AT-TMA-0.2-uncalcined, AT-TPA-0.2-uncalcined, and AT-CTA-0.2-uncalcined, were subjected to compositional analysis to get a more precise estimate of the amount of adsorbed PDA (**Table 3**). The resulting values (in wt.%) agreed well with the values depicted in **Fig. 6b**. Normalization to the zeolite content and molar mass of the ammonium cations yielded the molecular content of PDA per gram of zeolite. Taking these values and the surface area of an adsorbed PDA molecule ( $A_{\text{PDA}}$ ) into account [31], an estimation of the external surface area was made. Obviously, this estimation is most accurate assuming that the PDA molecules adsorb in a single layer fashion onto the zeolite's external surface. For samples AT-TPA-0.2-uncalcined

and AT-TPA-0.2-uncalcined similar predicted surface areas (*ca.* 500 m<sup>2</sup> g<sup>-1</sup>) were obtained, which relate reasonably to the values displayed in **Table 2**. Conversely, regarding AT-CTA-0.2-uncalcined, even assuming the smallest particle area on the zeolite's surface possible, the obtained mesopore surface area (820 m<sup>2</sup> g<sup>-1</sup>) largely exceeded the measured value for the calcined sample (591 m<sup>2</sup> g<sup>-1</sup>). This difference is attributed to the ability of CTA<sup>+</sup> to adsorb in a multilayer fashion to the surface [32], in contrast to the monolayer adsorption of TMA<sup>+</sup> and TPA<sup>+</sup> [14,33].

The porous properties displayed clear trends with the PDA concentration too. **Fig. 6c** shows that  $V_{\text{micro}}$  is largely preserved for TPA<sup>+</sup> and CTA<sup>+</sup> at  $c > 0.05$  M. The variation of the external surface area with the applied PDA concentration was quite pronounced. At  $c \geq 0.01$  M, mesopore areas exceeding 500 m<sup>2</sup> g<sup>-1</sup> were obtained for CTA<sup>+</sup> and TPA<sup>+</sup> (**Fig. 6d**). Irrespective on the applied concentration, TMA<sup>+</sup> was less suited, as it neither preserved the micropore volume, nor enhanced mesoporosity with an efficiency comparable to TPA<sup>+</sup> and CTA<sup>+</sup>.

Representative X-ray diffraction patterns clearly displayed preservation of the FAU structure for CTA-0.05 and TPA-0.2 (**Fig. 2a**). The retention of crystallinity became apparent for TPA<sup>+</sup> or CTA<sup>+</sup> using  $c > 0.01$  M (**Fig. 7a**). For TPA<sup>+</sup>, crystallinity plateaued around 85% at  $c > 0.05$  M, whereas for CTA<sup>+</sup> a maximum crystallinity of 50% was attained at 0.05 M. The molar Si/Al ratio of sample AT (19) and related yield (45%), show that the standard NaOH treatment without PDA was mostly selective to silicon. In contrast, in the presence of PDAs, the Si/Al ratio increased with its concentration to values similar to the parent zeolite (Si/Al = 32 for AT-CTA-0.2 and Si/Al = 35 for AT-TPA-0.2, **Fig. 7b**). This is ascribed to the adsorption of PDA on the zeolite, sealing off most of the available external surface, hereby largely inhibiting surface realumination. Accordingly, both Si and Al species are permanently leached from the zeolite. This means that, using 0.2 M of TPA<sup>+</sup> or CTA<sup>+</sup> in the alkaline solution, the term 'desilication' is no longer accurate in a broad sense: A more correct terminology would 'mesopore formation by base leaching'. The crystallinity and the Si/Al ratio of the TPA<sup>+</sup>-treated zeolites related well with the microporosity (insets of **Fig. 7**), highlighting the suitability of  $V_{\text{micro}}$  as descriptor for intrinsic zeolite properties.

An important result is that by varying the PDA concentration, the amount of realuminated Al can be controlled. This implies that, since these species typically display a pronounced (mostly Lewis) acidity [14,34,35], PDA-mediated base leaching enables to design zeolites with hierarchical porosity *and* hierarchical acidity. In the latter sense, the Brønsted acid sites located in the micropores are complemented with an auxiliary network of mesopores providing, besides an increased access, a secondary level of acidity. The latter may be of significance in tailoring hierarchical zeolites towards application in catalyzed reactions, *e.g.* fluid catalytic cracking [36]. Therefore, the in-depth study of the nature and location of realuminated Al species in hierarchical USY and beta zeolites is highly relevant. However, related efforts are beyond the scope of this contribution.

Based on the similar mesopore surface areas but higher microporosity, crystallinity, and Si/Al ratio, TPA<sup>+</sup> demonstrated a superior pore-directing agent compared to CTA<sup>+</sup>. This is attributed to a more ideal adsorption of the former cation, owing to its symmetrical and non-micelle forming nature [31]. In fact, the relatively low crystallinity and very narrow mesopore size distributions (at  $c = 0.05\text{-}0.2$  M) suggest that, during alkaline treatment with CTA<sup>+</sup>, a restructuring took place. The latter is supported by the applied moles of CTA<sup>+</sup> per gram of zeolite, particularly at 0.05 M and 0.1 M of CTA<sup>+</sup> (*ca.* 2 mmol g<sup>-1</sup>), being very similar to those reported in [20,21]. Nonetheless, unlike in [21], no low-angle peaks, typical of ordered mesopores, could be discerned in the XRD diffraction patterns of the AT-CTA- $c$  samples.

Besides influencing the crystallinity, microporosity, and the elemental composition, the PDA concentration also influences the mesopore size. **Fig. 5b** displays the isotherms derived from solids alkaline treated in the presence of 0.05, 0.1, and 0.2 M of DTA<sup>+</sup>. The isotherms display distinct uptakes at  $p/p_0 > 0.1$ , and **Fig. 6b** confirms the presence of various pore sizes, *i.e.* 8, 5, and 3 nm. Hence, the mesopore size can be tuned by selecting the right PDA *and* its concentration.

### 3.3. Extended characterization of selected samples

A more extensive study was performed on samples P, AT, AT-TPA-0.2, and AT-CTA-0.2. TEM shows that whereas standard desilication led to complete loss of crystallinity, the inclusion of TPA<sup>+</sup> or

CTA<sup>+</sup> in the alkaline solution led to the preservation of the lattice fringes (**Fig. 4**). The preservation of crystallinity was confirmed by SAED (insets in **Fig. 4**). Moreover, as opposed to the parent zeolite, no amorphous debris were identified in the micrographs of AT-TPA-0.2 and AT-CTA-0.2. TEM investigation did not reveal a secondary phase or any clear ordering of the mesopores in sample AT-CTA-0.2.

High-resolution low-pressure Ar adsorption was performed to more closely assess the influence of the treatments on the micropores (**Fig. 8**). The isotherms reveal that uptake of AT-TPA-0.2 and AT-CTA-0.2 at low relative pressures was similar to the parent zeolite. On the other hand, at  $p/p_0 > 0.1$ , the latter isotherms showed enhanced uptake, due to the presence of mesopores. The NLDFT pore size distributions confirm the large similarity of the micropore structures of P, AT-TPA-0.2, and AT-CTA-0.2. Plotted in the 0.5-20 nm range, the occurrence of a hierarchical pore system in the base-leached samples is unambiguously demonstrated.

Acidity assessment was performed by FT-IR spectroscopy in the OH stretching region. The IR spectrum of the parent sample displayed three main bands: at 3742 cm<sup>-1</sup>, representing the isolated surface silanols, and two bands at 3625 cm<sup>-1</sup> and 3560 cm<sup>-1</sup>, corresponding to the Brønsted acidic hydroxyls (**Fig. 9**). In addition, two shoulders at 3600 cm<sup>-1</sup> and 3545 cm<sup>-1</sup> were discerned, attributed to non-acidic hydroxyls formed by dealumination [37]. Upon standard alkaline treatment (AT), the band at 3742 cm<sup>-1</sup> increased strongly, attending to the increased external surface. However, the bands at 3625 cm<sup>-1</sup> and 3560 cm<sup>-1</sup> were absent, suggesting the loss of the Brønsted acidity, relating well with the complete loss of crystallinity. On the other hand, when either TPA<sup>+</sup> or CTA<sup>+</sup> was present in the alkaline solution the increase of the external surface, hence band at 3742 cm<sup>-1</sup>, was combined with a full preservation of bands related to Brønsted acidity. Also the shoulders at 3600 cm<sup>-1</sup> and 3545 cm<sup>-1</sup> remained apparent. In fact, all four bands in the 3500-3650 cm<sup>-1</sup> range appeared more intense than those related to the parent, which is, in line with the TEM observations, attributed to the presence of amorphous debris in P. These kind of debris tend to mask the bands of Brønsted acidic hydroxyls [13,25,38].

Skeletal density measurements by He pycnometry provided valuable insights into the implications of base leaching on the USY30 zeolite (**Table 4**). The helium density of sample P ( $2.26 \text{ g cm}^{-3}$ ) was somewhat lower than that of the pristine (non-dealuminated) Y zeolite ( $2.30 \text{ g cm}^{-3}$ , Y2.4-P). This was attributed to the presence of Si-rich debris, lowering the density towards a value typical for amorphous silica ( $2.05 \text{ g cm}^{-3}$ ). After standard alkaline treatment, the density reduced to  $2.16 \text{ g cm}^{-3}$ , which is surprising as the aluminum content had doubled and a value closer to a high surface area alumina ( $3.26 \text{ g cm}^{-3}$ ) may be expected. However, the value is explained by the intense amorphization of the sample, lowering the density towards a value typical of amorphous silica. Conversely, samples AT-TPA-0.2 and AT-CTA-0.2 comprised densities of *ca.*  $2.32 \text{ g cm}^{-3}$ , *i.e.* closer to the untreated NaY zeolite, which was, in agreement with TEM and IR techniques, attributed to the removal of debris present in P. The latter hypothesis is supported by the similar crystallinity evidenced for P (100%) and AT-TPA-0.2 (88%). Hence, whereas the introduction of mesoporosity is likely to reduce crystallinity, the removal of the amorphous species leads to an increased crystallinity, hereby reducing the net effect of the alkaline treatment.

### **3.4. Influence of aluminum content and framework**

The efficiency of PDAs to preserve intrinsic zeolite properties upon desilication was demonstrated on USY zeolites of distinct nominal Si/Al ratios, *i.e.* 15, 30, and 385. The parent USY zeolites comprised micropore volumes around  $0.30 \text{ cm}^3 \text{ g}^{-1}$  and mesopore surface areas of roughly  $115 \text{ m}^2 \text{ g}^{-1}$  (**Table 5**). Upon alkaline treatment, all USY zeolites (with or without PDA) displayed substantially enhanced mesopore surfaces (up to  $530 \text{ m}^2 \text{ g}^{-1}$ ). However,  $V_{\text{micro}}$  dropped dramatically upon standard NaOH treatment. Conversely, the inclusion of 0.01 M of CTA<sup>+</sup> in the alkaline solution led to the preservation of the micropore volume, emphasizing the broad applicability of these PDAs in base leaching of USY zeolites for mesopore formation. Most likely, the porous properties of the treated zeolites presented in this section could be further optimized by tailoring the type and concentration of applied PDA. However, the associated additional screening goes beyond the scope of this contribution.

Like USY zeolites, also beta zeolites easily amorphize when exposed to alkaline aqueous solutions [39]. Accordingly, various authors reported distinct ways to introduce mesopores by desilication, while minimizing amorphization: by using very mild conditions [39], by applying an organic base such as TMAOH [11], or by partially detemplating the zeolite prior to treatment [40]. The parent beta zeolite (beta220-P) used in this study comprised a very high nominal Si/Al ratio of 220, implying an even higher sensitivity in alkaline media compared to beta zeolites described in the above-mentioned studies. The XRD pattern displayed the reflections archetypal of a pure beta zeolite (**Fig. 2b**). Like in the case of the USY30 zeolite, NaOH treatment (beta220-AT) completely amorphized the sample, judging from the absence of reflections in the pattern. In contrast, when 0.01 M CTA<sup>+</sup> was included in the alkaline solution (beta220-AT-CTA-0.01), about 85% of crystallinity relative to the parent beta zeolite was maintained.

The N<sub>2</sub> isotherm of beta220-P displayed uptake most notably at low relative pressures (**Fig. 10**). Application of the *t*-plot method led to a  $V_{\text{micro}} = 0.20 \text{ cm}^3 \text{ g}^{-1}$  and a  $S_{\text{meso}} = 82 \text{ m}^2 \text{ g}^{-1}$ . The NaOH treatment (beta220-AT) induced an increase in uptake at  $p/p_0 > 0.1$  in the N<sub>2</sub> isotherm, but concomitantly originated a substantial loss of the uptake at low relative pressures. Accordingly, the mesopore surface area increased to  $236 \text{ m}^2 \text{ g}^{-1}$ , but the  $V_{\text{micro}}$  dropped to zero (**Table 5**). Following the strategy applied to the USY zeolites, beta220-AT-CTA-0.01 exhibited a largely preserved micropore volume ( $V_{\text{micro}} = 0.14 \text{ cm}^3 \text{ g}^{-1}$ ) and a strongly enhanced external surface area ( $S_{\text{meso}} = 477 \text{ m}^2 \text{ g}^{-1}$ ), *i.e.* almost six-fold that of the parent beta220 zeolite. Interestingly, whereas the isotherm of beta220-AT-CTA-0.01 is shifted upwards by *ca.*  $50 \text{ cm}^3 \text{ g}^{-1}$  from beta220-P, the obtained micropore volume using the *t*-plot was 30% lower. Argon adsorption at 77 K was employed to more precisely assess the influence of the treatment on the microporosity (**Fig. 11**). The resulting isotherms, derived NLDFT pore size distributions, and cumulative pore volumes, demonstrated a superior micropore volume of beta220-AT-CTA-0.01 over that of the parent beta zeolite. Accordingly, it may be obvious that the *t*-plot method is not the most precise method to determine the microporosity of hierarchical zeolites.



### 3.5. Continuous preparation of hierarchical zeolites

The synthesis of mesoporous zeolites by alkaline treatment has thus far been restricted to batch operation. Although providing obvious advantages on the lab scale, the batch process does not provide optimal reactor productivity, relevant to an industrial context [41]. By using a high-shear micro-reactor or a tubular reactor (**Fig. 1**), productivity can be increased and, advantageously, in-line separation is facilitated. We performed desilication in the continuous mode co-feeding a solution of NaOH and TPABr and a suspension of zeolite to an in-line high-shear disperser under various conditions (**Table 6**). These experiments yielded productivities of 33 and 110 g L<sup>-1</sup> min<sup>-1</sup>, *i.e.* about 30 and 100 times higher than a typical batch alkaline treatment (1 g L<sup>-1</sup> min<sup>-1</sup>). The external surfaces of the resulting solids were significant (> 300 m<sup>2</sup> g<sup>-1</sup>) and approached the value obtained using the batch process (438 m<sup>2</sup> g<sup>-1</sup>). The porosities of the resulting solids were tunable by variation of the flowrate ( $Q$ ), stirring speed ( $\omega$ ), and NaOH concentration. Unsurprisingly, using the high-shear micro-reactor, stirring proved essential, as co-feeding the solutions through an un-stirred chamber did not lead to the introduction of substantial mesoporosity. Nevertheless, in the absence of stirring, the introduction of mesoporosity was enabled by using a tubular reactor, hence longer residence time, and heating. Obviously, in this case productivity reduced to 2 g L<sup>-1</sup> min<sup>-1</sup>.

## 4. Conclusions

The use of pore-directing agents in NaOH leaching is demonstrated as a generic approach to introduce extensive intra-crystalline mesoporosity in USY and beta zeolites, while preserving the intrinsic zeolite properties, *e.g.* microporosity, crystallinity, and composition. While a wide variety of organic molecules display a pore-directing role, efficient PDAs are positively charged and have organic moieties in the range of *ca.* 10-20 carbon atoms. Of the evaluated molecular species, TPA<sup>+</sup> yields highly mesoporous zeolites with intrinsic zeolite properties closest to the parent zeolite. CTA<sup>+</sup>, on the other hand, combines the introduction of mesoporosity and preservation of intrinsic zeolite properties with a facilitated reassembly of leached species. Alkaline treatment in the presence of PDAs enabled the

removal of amorphous debris present in steamed and acid-leached USY zeolites. The measurement of skeletal densities demonstrated of high potential unraveling the species formed upon post-synthetic modifications of zeolites. Last but not least, we report the first-time synthesis of mesoporous zeolites in continuous mode. This achievement further highlights the amenability of base leaching to prepare hierarchical zeolites in an industrial context.

**Acknowledgment.** The Swiss National Science Foundation (project number 200021-134572) is acknowledged. We thank Dr. F. Krumeich for the electron microscopic analyses. The Electron Microscopy Centre of the Swiss Federal Institute of Technology (EMEZ) is acknowledged for use of their facilities.

## References

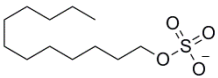
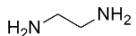
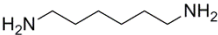
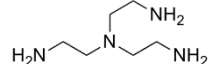
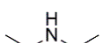

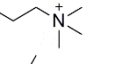
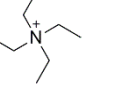
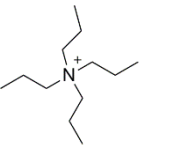
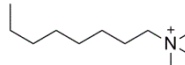
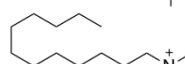
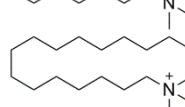
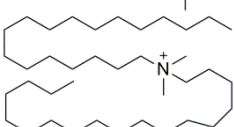
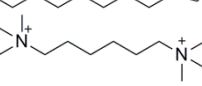
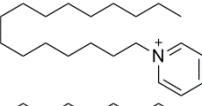
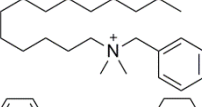
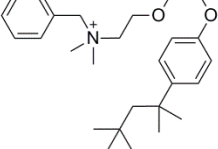
- [1] Corma, A. *Chem. Rev.* **1995**, *95*, 559.
- [2] Vermeiren, W.; Gilson, J. -P. *Top. Catal.* **2009**, *52*, 1131.
- [3] Jiang, J.; Jorda, J. L.; Yu, J.; Baumes, L. A.; Mugnaioli, E.; Díaz-Cabañas, M. J.; Kolb, U.; Corma, A. *Science*, **2011**, *333*, 1131.
- [4] Inayat, A.; Knoke, I.; Spiecker, E.; Schwieger W. *Angew. Chem. Int. Ed.* **2012**, *51*, 1962.
- [5] Ng, E. -P.; Chateigner, D.; Bein, T.; Valtchev, V.; Mintova, S. *Science*, **2012**, *335*, 70.
- [6] Egeblad, K.; Christensen, C. H.; Kustova, M.; Christensen, C. H. *Chem. Mater.* **2008**, *20*, 946.
- [7] Verboekend, D.; Pérez-Ramírez, J. *Catal. Sci. Technol.* **2011**, *1*, 879.
- [8] Pérez-Ramírez, J.; Christensen, C. H.; Egeblad, K.; Christensen, C. H.; Groen, J. C. *Chem. Soc. Rev.* **2008**, *37*, 2530.
- [9] Chal, R.; Gérardin, C.; Bulut, M.; van Donk, S. *ChemCatChem* **2011**, *3*, 67.
- [10] Lopez-Orozco, S.; Inayat, A.; Schwab, A.; Selvam, T.; Schwieger, W. *Adv. Mater.* **2011**, *23*, 2602.
- [11] Holm, M. S.; Hansen, M. K.; Christensen, C. H. *Eur. J. Inorg. Chem.* **2009**, 1194.

- [12] Pérez-Ramírez, J.; Verboekend, D.; Bonilla, A.; Abelló, S. *Adv. Funct. Mater.* **2009**, *19*, 3972.
- [13] Verboekend, D.; Vilé, G.; Pérez-Ramírez, J. *Adv. Funct. Mater.* **2012**, *22*, 916.
- [14] Verboekend, D.; Pérez-Ramírez, J. *Chem. Eur. J.* **2011**, *17*, 1137.
- [15] Gu, F. N.; Wei, F.; Yang, J. Y.; Lin, N.; Lin, W. G.; Wang, Y.; Zhu, J. H. *Chem. Mater.* **2010**, *22*, 2442.
- [16] Zhu, Y.; Hua, Z.; Zhou, J.; Wang, L.; Zhao, J.; Gong, Y.; Wu, W.; Ruan, M.; Shi, J. *Chem. Eur. J.* **2011**, *17*, 14618.
- [17] Inagaki, S.; Ogura, M.; Inami, T.; Sasaki, Y.; Kikuchi, E.; Matsukata, M. *Microporous Mesoporous Mater.* **2004**, *74*, 163.
- [18] Khitev, Yu. P.; Kolyagin, Yu. G.; Ivanova, I. I.; Ponomareva, O. A.; Thibault-Starzyk, F.; Gilson, J. -P.; Fernandez, C.; Fajula, F. *Microporous Mesoporous Mater.* **2011**, *146*, 201.
- [19] Chal, R.; Cacciaguerra, T.; van Donk, S.; Gérardin, C. *Chem. Commun.* **2010**, *46*, 7840.
- [20] Yoo, W. C.; Zhang, X.; Tsapatsis, M.; Stein, A. *Microporous Mesoporous Mater.* **2012**, *149*, 147.
- [21] García-Martínez, J.; Johnson, M.; Valla, J.; Li, K.; Ying, J. Y. *Catal. Sci. Technol.* **2012**, *2*, 987.
- [22] Janssen, A. H.; Koster, A. J.; de Jong, K. P. *J. Phys. Chem. B* **2002**, *106*, 11905.
- [23] Lutz, W.; Kurzhals, R.; Kryukova, G.; Enke, D.; Weber, M.; Heidemann, D. *Z. Anorg. Allg. Chem.* **2010**, *636*, 1497.
- [24] Verboekend, D.; Chabaneix, A. M.; Thomas, K.; Gilson, J. -P.; Pérez-Ramírez, J. *CrystEngComm*, **2011**, *13*, 3408.
- [25] Verboekend, D.; Mitchell, S.; Milina, M.; Groen, J. C.; Pérez-Ramírez, J. *J. Phys. Chem. C* **2011**, *115*, 14193.
- [26] Baerlocher, C.; McCusker, L. B.; Database of Zeolite Structures, <http://www.izastructure.org/databases>.
- [27] Ernst, S.; Weitkamp, J.; Martens, J. A.; Jacobs, P. A. *Appl. Catal.* **1989**, *48*, 137.

- [28] Rollmann, L. D.; Schlenker, J. L.; Lawton, S. L.; Kennedy, C. L.; Kennedy, G. J.; Doren, D. J. *J. Phys. Chem. B* **1999**, *102*, 7175.
- [29] van der Donck, J. C. J.; Vaessen, G. E. J.; Stein, H. N. *Langmuir* **1993**, *9*, 3553.
- [30] Choi, M.; Cho, H. S.; Srivastava, R.; Venkatesan, C.; Choi, D. -H.; Ryoo, R. *Nat. Mater.* **2006**, *5*, 718.
- [31] Claesson, P.; Horn, R. G.; Pashley, R. M. *J. Colloid Interf. Sci.* **1984**, *100*, 250.
- [32] Grosse, I.; Estel, K. *Colloid Polym. Sci.* **2000**, *278*, 1000.
- [33] Li, X.; Shantz, D. F. *J. Phys. Chem. C* **2010**, *114*, 8449.
- [34] Holm, M. S.; Svelle, S.; Joensen, F.; Beato, P.; Christensen, C. H.; Bordiga, S.; Bjørgen, M. *Appl. Catal. A* **2009**, *356*, 23.
- [35] Fernandez, C.; Stan, I.; Gilson, J. -P.; Thomas, K.; Vicente, A.; Bonilla, A.; Pérez-Ramírez, J. *Chem. Eur. J.* **2010**, *16*, 6224.
- [36] Mann, R. *Catal. Today* **1993**, *18*, 509.
- [37] Jacobs, P.; Uytterhoeven, J. B. *J. Catal.* **1971**, *22*, 193.
- [38] Corma, A.; Fornés, V.; Rey, F. *Appl. Catal.* **1990**, *59*, 267.
- [39] Groen, J. C.; Abelló, S.; Villaescusa, L. A.; Pérez-Ramírez, J. *Microporous Mesoporous Mater.* **2008**, *114*, 93.
- [40] Pérez-Ramírez, J.; Abelló, S.; Bonilla, A.; Groen, J. C. *Adv. Funct. Mater.* **2009**, *19*, 164.
- [41] van Gerven, T.; Stankiewicz, A. *Ind. Eng. Chem. Res.* **2009**, *48*, 2465.

## Tables

**Table 1.** Molecules tested as pore-directing agents in the NaOH treatment.

| Acronym               | Name                      | Type/structure  | Chemical formula   | Counterion        |
|-----------------------|---------------------------|---|--|-------------------|
| Anionic surfactant    |                           |   |  |                   |
| DS <sup>-</sup>       | Dodecylsulfate            |    | CH <sub>3</sub> (CH <sub>2</sub> ) <sub>11</sub> OSO <sub>3</sub> <sup>-</sup>   | Na <sup>+</sup>   |
| Non-ionic surfactants |                           |   |  |                   |
| P123                  | Pluronic P-123            | Polymer   | HO(CH <sub>2</sub> CH <sub>2</sub> O) <sub>20</sub> -<br>(CH <sub>2</sub> CH(CH <sub>3</sub> )O) <sub>70</sub> -<br>(CH <sub>2</sub> CH <sub>2</sub> O) <sub>20</sub> H  | -                 |
| EDA                   | Ethylenediamine           |    | C <sub>2</sub> H <sub>4</sub> (NH <sub>2</sub> ) <sub>2</sub>  | -                 |
| DAH                   | Diaminohexane             |    | H <sub>2</sub> N(CH <sub>2</sub> ) <sub>6</sub> NH <sub>2</sub>  | -                 |
| TAEA                  | Trisaminoethylamine       |    | N(CH <sub>2</sub> CH <sub>2</sub> NH <sub>2</sub> ) <sub>3</sub>   | -                 |
| DEA                   | Diethylamine              |    | HN(CH <sub>2</sub> CH <sub>3</sub> ) <sub>2</sub>  | -                 |
| Cationic surfactants  |                           |   |  |                   |
| TMA <sup>+</sup>      | Tetramethylammonium       |    | N <sup>+</sup> (CH <sub>3</sub> ) <sub>4</sub>   | Br <sup>-</sup>   |
| PTA <sup>+</sup>      | Propyltrimethylammonium   |    | (CH <sub>3</sub> ) <sub>3</sub> N <sup>+</sup> C <sub>3</sub> H <sub>7</sub>   | Br <sup>-</sup>   |
| TEA <sup>+</sup>      | Tetraethylammonium        |    | N <sup>+</sup> (C <sub>2</sub> H <sub>5</sub> ) <sub>4</sub>   | Br <sup>-</sup>   |
| TPA <sup>+</sup>      | Tetrapropylammonium       |   | N <sup>+</sup> (C <sub>3</sub> H <sub>7</sub> ) <sub>4</sub>   | Br <sup>-</sup>   |
| OTA <sup>+</sup>      | Octyltrimethylammonium    |  | (CH <sub>3</sub> ) <sub>3</sub> N <sup>+</sup> C <sub>8</sub> H <sub>17</sub>  | Br <sup>-</sup>   |
| DTA <sup>+</sup>      | Dodecyltrimethylammonium  |  | (CH <sub>3</sub> ) <sub>3</sub> N <sup>+</sup> C <sub>12</sub> H <sub>25</sub>   | Br <sup>-</sup>   |
| CTA <sup>+</sup>      | Cetyltrimethylammonium    |  | (CH <sub>3</sub> ) <sub>3</sub> N <sup>+</sup> C <sub>16</sub> H <sub>33</sub>   | Br <sup>-</sup>   |
| DSA <sup>+</sup>      | Dimethyldistearylammonium |  | (C <sub>18</sub> H <sub>37</sub> ) <sub>2</sub> N <sup>+</sup> (CH <sub>3</sub> ) <sub>2</sub>   | Cl <sup>-</sup>   |
| HM <sup>2+</sup>      | Hexamethonium             |  | (CH <sub>3</sub> ) <sub>3</sub> N <sup>+</sup> C <sub>6</sub> H <sub>12</sub> N <sup>+</sup> (CH <sub>3</sub> ) <sub>3</sub>   | 2 Br <sup>-</sup> |
| HDP <sup>+</sup>      | Hexadecylpyridinium       |  | C <sub>16</sub> H <sub>33</sub> N <sup>+</sup> C <sub>5</sub> H <sub>5</sub>   | Cl <sup>-</sup>   |
| BA <sup>+</sup>       | Benzalkonium              |  | C <sub>6</sub> H <sub>5</sub> CH <sub>2</sub> N <sup>+</sup> (CH <sub>3</sub> ) <sub>2</sub> R,<br>R = C <sub>8</sub> H <sub>17</sub> to C <sub>16</sub> H <sub>33</sub>   | Br <sup>-</sup>   |
| BE <sup>+</sup>       | Benzethonium              |  | C <sub>6</sub> H <sub>5</sub> CH <sub>2</sub> N <sup>+</sup> (CH <sub>3</sub> ) <sub>2</sub> -<br>C <sub>2</sub> H <sub>2</sub> OC <sub>2</sub> H <sub>2</sub> O<br>C <sub>6</sub> H <sub>4</sub> C(CH <sub>3</sub> ) <sub>2</sub> CH <sub>2</sub> C-<br>(CH <sub>3</sub> ) <sub>2</sub> CH <sub>3</sub> | Cl <sup>-</sup>   |

**Table 2.** Porous properties of USY30 zeolites alkaline treated in the presence of various PDAs.

| Sample        | Yield (%) | $V_{\text{micro}}^{\text{a}}$ ( $\text{cm}^3 \text{g}^{-1}$ ) | $V_{\text{pore}}^{\text{b}}$ ( $\text{cm}^3 \text{g}^{-1}$ ) | $S_{\text{meso}}^{\text{a}}$ ( $\text{m}^2 \text{g}^{-1}$ ) | $d_{\text{p}}^{\text{c}}$ (nm) | $\text{DE}^{\text{d}}$ ( $\text{m}^2 \text{g}^{-1} \%^{-1}$ ) | IHF <sup>e</sup> (-) |
|---------------|-----------|---|--|---|--------------------------------|---|----------------------|
| P             | -         | 0.33  | 0.61   | 117   | -                              | -   | 0.16                 |
| AT            | 44        | 0   | 0.58   | 321   | 5                              | 4   | 0                    |
| AT-DS-0.2     | 43        | 0   | 0.35   | 144   | 7                              | 1   | 0                    |
| AT-P123-0.005 | 53        | 0.07  | 0.85   | 324   | 13                             | 4   | 0.09                 |
| AT-EDA-0.2    | 45        | 0   | 0.68   | 466   | 5                              | 6   | 0                    |
| AT-DAH-0.2    | 35        | 0.09  | 0.85   | 498   | 6                              | 6   | 0.19                 |
| AT-TAEA-0.2   | 63        | 0.14  | 0.56   | 270   | 4                              | 4   | 0.16                 |
| AT-DEA-0.2    | 37        | 0.17  | 1.18   | 483   | 12                             | 6   | 0.34                 |
| AT-TMA-0.2    | 58        | 0.11  | 0.75   | 476   | 4                              | 9   | 0.22                 |
| AT-PTA-0.2    | 53        | 0.12  | 0.94   | 584   | 7                              | 10  | 0.29                 |
| AT-TEA-0.2    | 52        | 0.15  | 1.01   | 593   | 6                              | 10  | 0.37                 |
| AT-TPA-0.2    | 56        | 0.28  | 1.18   | 578   | 7                              | 11  | 0.67                 |
| AT-OTA-0.2    | 61        | 0.23  | 0.90   | 426   | 5                              | 8   | 0.41                 |
| AT-DTA-0.2    | 60        | 0.26  | 0.90   | 425   | 3                              | 8   | 0.46                 |
| AT-CTA-0.2    | 50        | 0.22  | 1.02   | 591   | 4                              | 10  | 0.54                 |
| AT-DSA-0.2    | 63        | 0.15  | 1.13   | 733   | 6                              | 12  | 0.45                 |
| AT-HM-0.2     | 61        | 0.18  | 1.01   | 591   | 5                              | 12  | 0.44                 |
| AT-HDP-0.2    | 66        | 0.24  | 0.86   | 530   | 4                              | 12  | 0.53                 |
| AT-BA-0.2     | 67        | 0.26  | 0.83   | 380   | 4                              | 8   | 0.41                 |
| AT-BE-0.2     | 50        | 0.27  | 0.87   | 439   | 3                              | 6   | 0.49                 |

<sup>a</sup> $t$ -plot method. <sup>b</sup>Volume adsorbed at  $p/p_0 = 0.99$ . <sup>c</sup>Average BJH mesopore size. <sup>d</sup>Desilication efficiency. <sup>e</sup>Indexed hierarchy factor.

**Table 3.** Quantification of pore-directing agents adsorbed on selected samples.

| Sample                | PDA <sub>ads</sub> (wt.%) <sup>a</sup> | PDA <sub>ads</sub> (mmol g <sup>-1</sup> ) <sup>a,b</sup> | A <sub>PDA</sub> (nm <sup>2</sup> ) <sup>c</sup> | predicted <i>S</i> <sub>meso</sub> (m <sup>2</sup> g <sup>-1</sup> ) |
|-----------------------|--|---|--|--|
| AT-TMA-0.2-uncalcined | 11                                     | 1.7   | 0.54   | 540  |
| AT-TPA-0.2-uncalcined | 17                                     | 1.1   | 0.77   | 523  |
| AT-CTA-0.2-uncalcined | 42                                     | 2.5   | 0.54 <sup>d</sup>                                | 840  |

<sup>a</sup>Elemental analysis. <sup>b</sup>mmol PDA per gram of zeolite. <sup>c</sup>Surface area per adsorbed PDA molecule [31]. <sup>d</sup>Area assuming an equivalent surface coverage for CTA<sup>+</sup> and TMA<sup>+</sup>.

**Table 4.** Skeletal densities of selected samples.

| Sample                         | $\rho_s$ (g cm <sup>-3</sup> ) |
|--------------------------------|--------------------------------|
| P                              | 2.26                           |
| AT                             | 2.16                           |
| AT-TPA-0.2                     | 2.31                           |
| AT-CTA-0.2                     | 2.34                           |
| Y2.4-P                         | 2.30                           |
| SiO <sub>2</sub>               | 2.05                           |
| Al <sub>2</sub> O <sub>3</sub> | 3.26                           |



**Table 5.** Porous properties of USY and beta zeolites.

| Sample  | $V_{\text{micro}} \text{ (cm}^3 \text{ g}^{-1}\text{)}$ |      |             | $S_{\text{meso}} \text{ (m}^2 \text{ g}^{-1}\text{)}$ |     |             |
|---------|---|------|-------------|---|-----|-------------|
|         | P   | AT   | AT-CTA-0.01 | P   | AT  | AT-CTA-0.01 |
| USY15   | 0.28  | 0.04 | 0.23        | 125   | 275 | 240         |
| USY30   | 0.33  | 0    | 0.22        | 117   | 321 | 496         |
| USY385  | 0.30  | 0.02 | 0.26        | 100   | 530 | 207         |
| beta220 | 0.20  | 0    | 0.14        | 82  | 236 | 477         |

**Table 6.** Properties of USY30 zeolites alkaline treated in the continuous and batch mode.

| Mode                       | $\omega$<br>(rpm) | $Q$<br>(cm <sup>3</sup> min <sup>-1</sup> ) | [NaOH] <sup>a</sup><br>(M) | $\tau$ <sup>b</sup><br>(s) | $V_{\text{micro}}$<br>(cm <sup>3</sup> g <sup>-1</sup> ) | $V_{\text{pore}}$<br>(cm <sup>3</sup> g <sup>-1</sup> ) | $S_{\text{meso}}$<br>(m <sup>2</sup> g <sup>-1</sup> ) |
|----------------------------|-------------------|---|----------------------------|----------------------------|--|---|--|
| Continuous-HS <sup>c</sup> | 13500             | 20  | 0.2                        | 18                         | 0.27   | 0.74  | 309  |
| Continuous-HS              | 13500             | 6   | 0.2                        | 60                         | 0.24   | 0.85  | 427  |
| Continuous-HS              | 24000             | 20  | 0.2                        | 18                         | 0.28   | 0.77  | 325  |
| Continuous-HS              | 13500             | 20  | 0.4                        | 18                         | 0.24   | 0.81  | 365  |
| Continuous-HS              | -                 | 20  | 0.2                        | 18                         | 0.34   | 0.65  | 166  |
| Continuous-T <sup>d</sup>  | -                 | 10  | 0.2                        | 900                        | 0.24   | 0.84  | 361  |
| Batch                      | 500               | -   | 0.2                        | 1800                       | 0.20   | 0.96  | 438  |

<sup>a</sup>In all cases, TPA<sup>+</sup> (0.05 M) was used as PDA. <sup>b</sup>Residence time. <sup>c</sup>High-shear micro-reactor.

<sup>d</sup>Tubular reactor.

## Figure captions

**Figure 1.** Set-ups to perform alkaline treatments: (a) batch reactor, (b) continuous tubular reactor, and (c) continuous high-shear micro-reactor.

**Figure 2.** X-ray diffraction patterns of (a) USY30 and (b) beta220 zeolites.

**Figure 3.** Scanning electron micrographs of USY30 zeolites. The scale bar applies to both micrographs.

**Figure 4.** Transmission electron micrographs of USY30 zeolites. The dashed lines indicate the presence of amorphous debris in the parent USY30 sample. The scale bar applies to all micrographs. Insets: selected area diffraction patterns.

**Figure 5.** (a, b) N<sub>2</sub> isotherms of USY30 zeolites. The arrow highlights the increased uptake at low relative pressures due to the inclusion of pore-directing agents in the alkaline solutions. (c, d) BJH mesopore size distributions derived from the isotherms in (a, b).

**Figure 6.** Variation of (a) yield, (b) adsorbed pore-directing agent after the alkaline treatment (PDA<sub>ads</sub>), (c) micropore volume, and (d) mesopore surface area of USY30 zeolites with the PDA concentration during NaOH treatment. The 'c' in the legend refers to the PDA concentration.

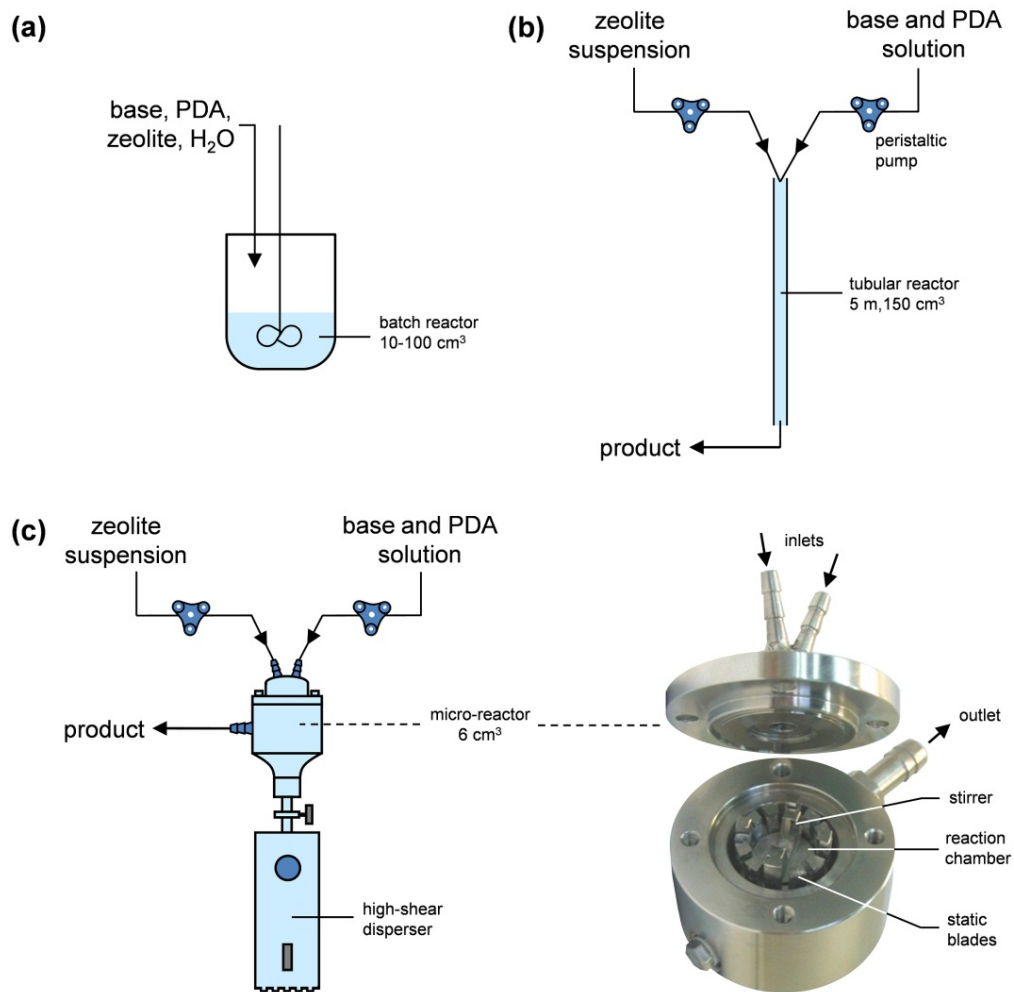
**Figure 7.** Variation of (a) crystallinity and (b) molar Si/Al ratio of USY30 zeolites with the concentration of TPA<sup>+</sup> or CTA<sup>+</sup> during NaOH treatment. The 'c' in the legend refers to the TPA<sup>+</sup> or CTA<sup>+</sup> concentration. Insets: crystallinity and the Si/Al ratio plotted as a function of the micropore volume.

**Figure 8.** (a) Ar isotherms at 87 K of USY30 zeolites and (b, c) derived NLDFT pore size distributions.

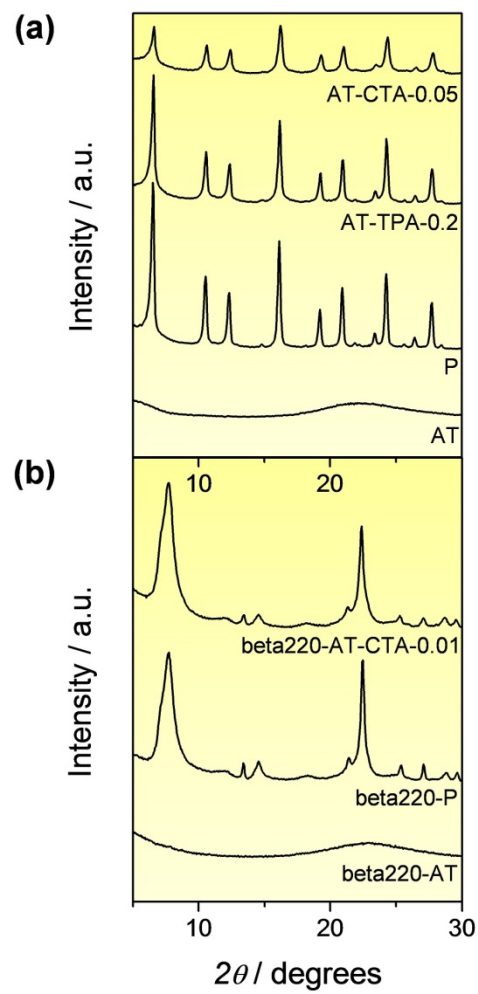
**Figure 9.** Infrared spectra in the OH stretching region of USY30 zeolites.

**Figure 10.** N<sub>2</sub> isotherms of beta220 zeolites. The arrow highlights the increased uptake at low relative pressures due to the inclusion of 0.01 M CTA<sup>+</sup> in the alkaline solution. Inset: BJH mesopore size distributions.

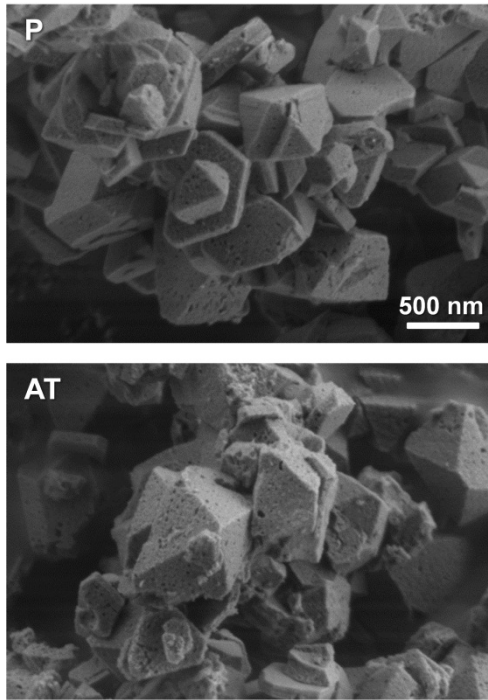
**Figure 11.** (a) Ar isotherms at 77 K of selected beta zeolites, (b) derived NLDFT pore size distributions, and (c) the cumulative pore volume as a function of the pore size. All three graphs demonstrate a superior microporosity of sample beta220-CTA-0.01 over that of the parent zeolite (beta220-P).



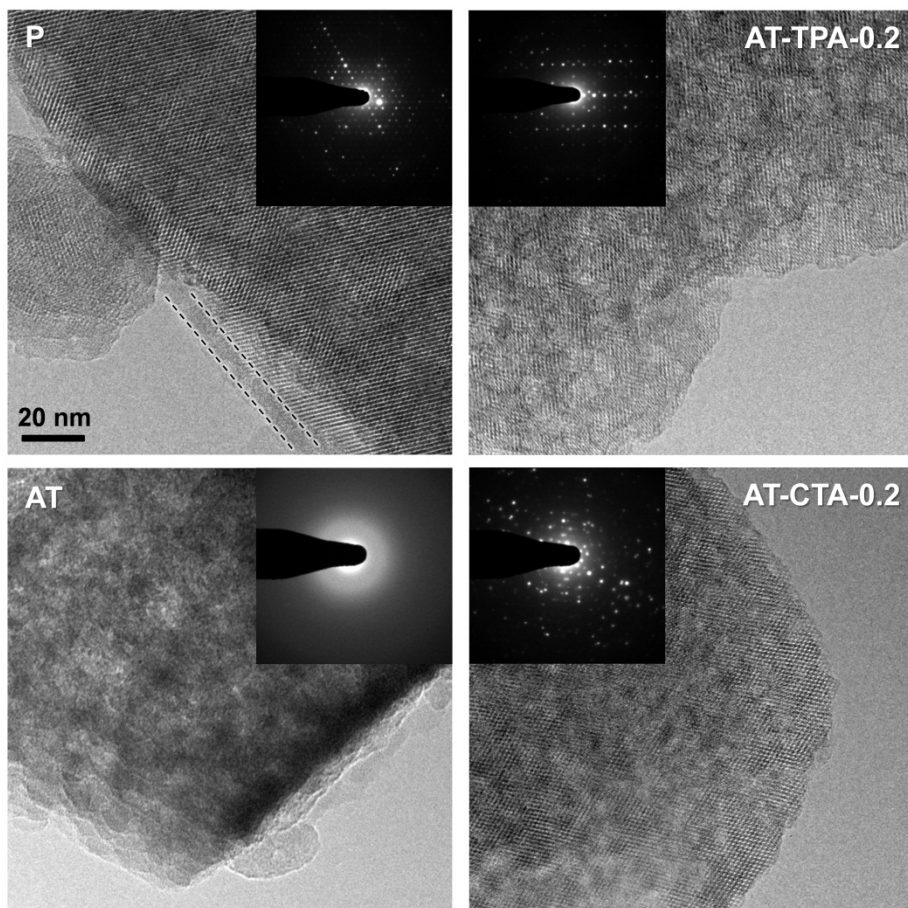
**Figure 1**



**Figure 2**



**Figure 3**



**Figure 4**



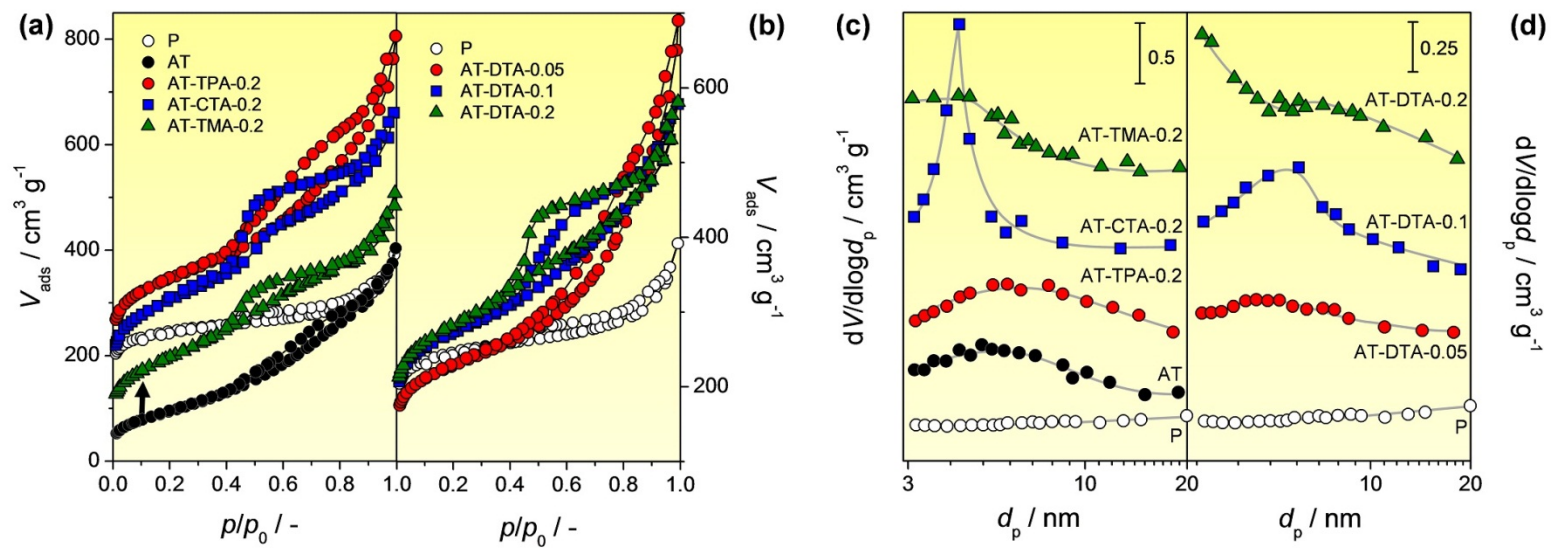


Figure 5

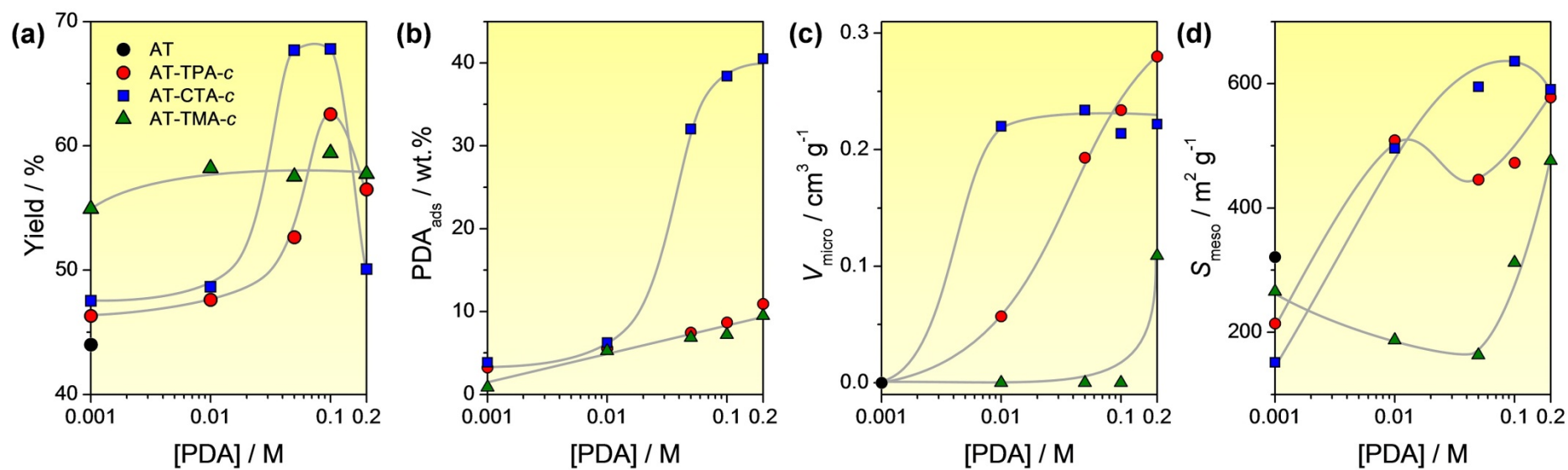


Figure 6

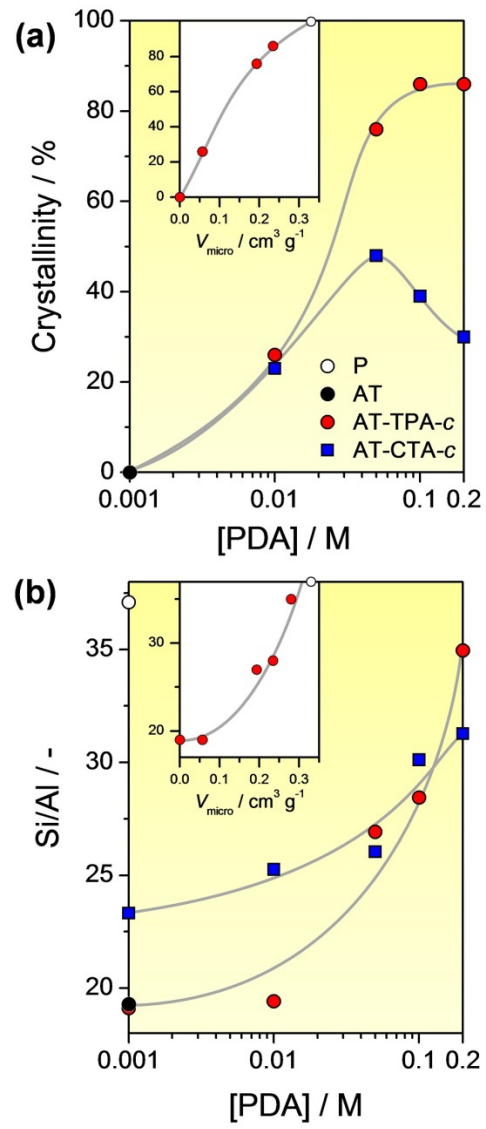


Figure 7

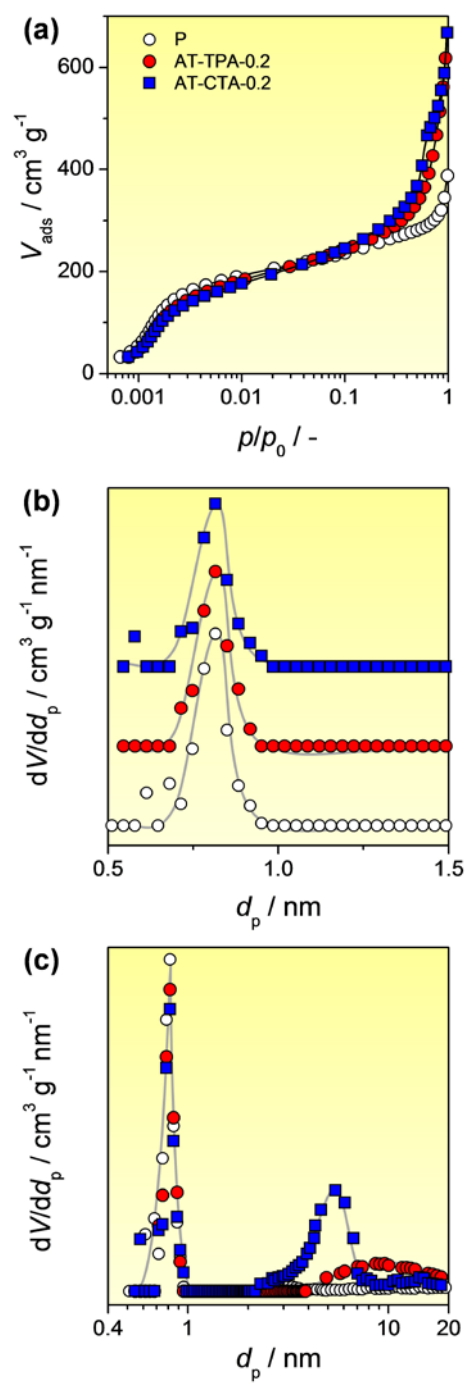
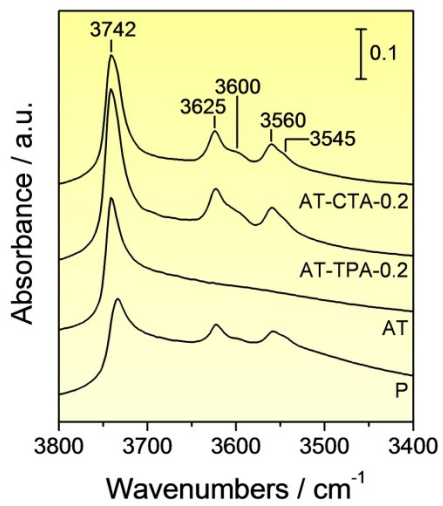
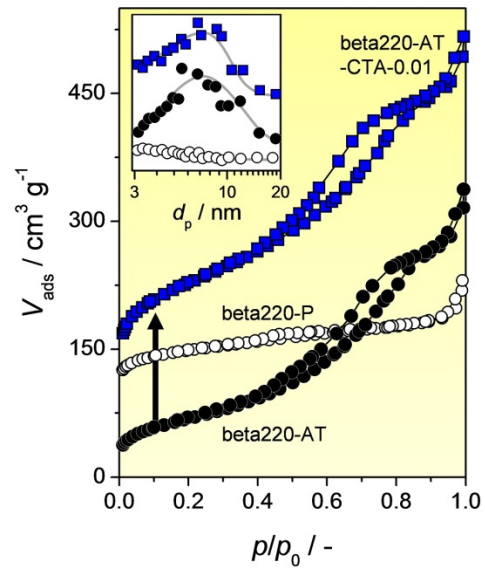


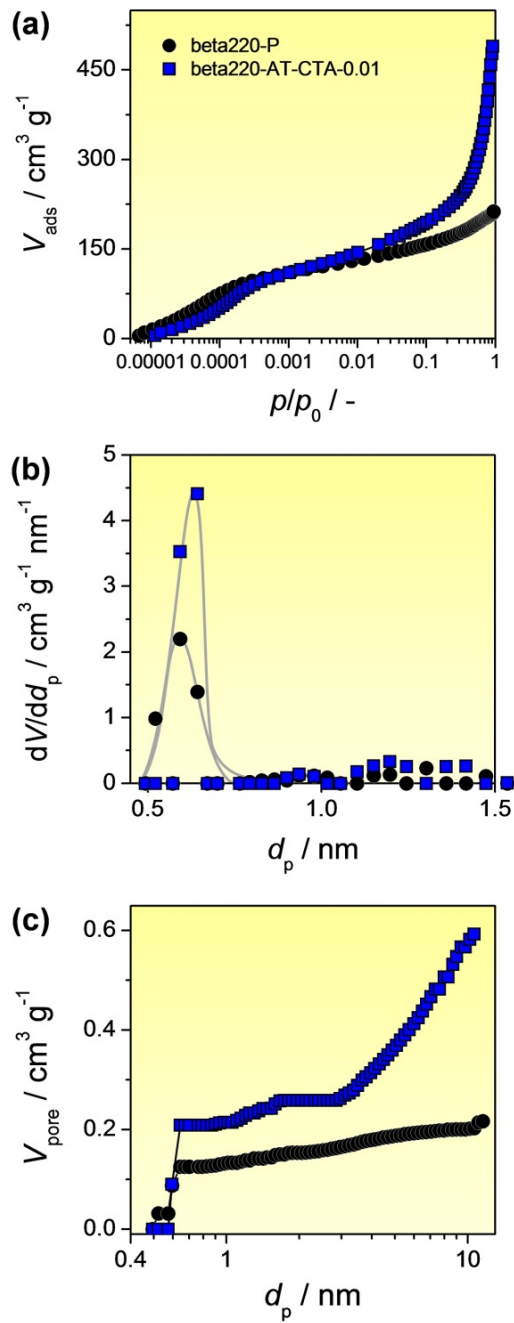
Figure 8



**Figure 9**

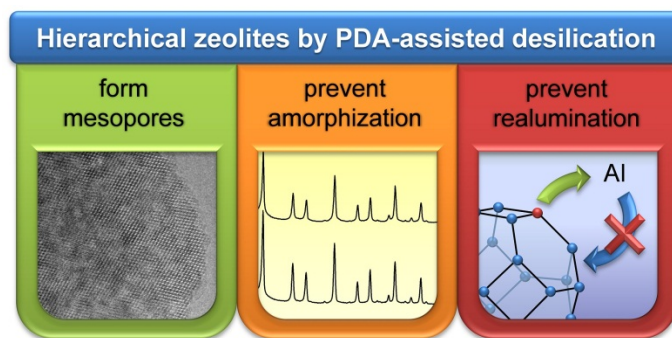


**Figure 10**



**Figure 11**

## Table of Contents graphic with the synopsis



The inclusion of pore-directing agents in the NaOH leaching of USY and beta zeolites enables extensive intra-crystalline mesopore formation while preventing amorphization and realumination.